IEEE Access
Multidisciplinary | Rapid Review | Open Access Journal

Received March 4, 2019, accepted March 26, 2019, date of publication April 4, 2019, date of current version April 24, 2019.

Digital Object Identifier 10.1109/ACCESS.2019.2909489

Modeling of Semiconductor Electrostatic Qubits Realized Through Coupled Quantum Dots

PANAGIOTIS GIOUNANLIS[1], (Member, IEEE), ELENA BLOKHINA[1], (Senior Member, IEEE), KRZYSZTOF POMORSKI[1], DIRK R. LEIPOLD[2], (Member, IEEE), AND ROBERT BOGDAN STASZEWSKI[1,2], (Fellow, IEEE)

[1]School of Electrical and Electronic Engineering, University College Dublin, Dublin 4, Ireland
[2]Equal1 Labs, Fremont, CA 94536, USA

Corresponding author: Elena Blokhina (elena.blokhina@ucd.ie)

This work was supported by the Science Foundation Ireland under Grant 14/RP/I2921.

ABSTRACT Considering the enormous advances in nanometer-scale CMOS technology that now allows one to reliably fabricate billions of switching devices on a single silicon die, electrostatically controlled quantum dots (implemented as quantum wells) appear to be promising candidates for a massive implementation of quantum bits (qubits) and quantum logic circuits in order to facilitate high-volume production of quantum computers. In this paper, the case of finite two-well and multiple-well potentials arising from semiconductor charged-coupled structures are treated in a rigorous way by Schrödinger formalism. The modeling methodologies presented to allow one to describe the dynamics of quantum states in non-ideal geometries, account for some mechanisms of qubit decoherence and model electrostatic interaction between electrons that lead to entanglement. The presented methodology can be scaled up to circuits of greater complexity.

INDEX TERMS CMOS technology, electrostatic semiconductor qubit, coupled semiconductor quantum dot, *N*-well system, decoherence time, time-dependent Schrödinger equation, predictor-corrector scheme, occupancy oscillations, tight-binding method, entanglement, entangled electrons, quantum computer.

I. INTRODUCTION

The race towards the implementation of a practical quantum computer is taking place worldwide as D-wave, Google, IBM, Intel, Microsoft, and other companies intensify their efforts. At this stage of technology, the first quantum computers can sustain a few dozen quantum bits (qubits). Quantum computers can deliver an exponential computational processing boost by overcoming the performance limitations of classical computers [1], [2]. This spurs fundamental research related to the massive operation of qubits [3], [4]. It is not surprising that physical systems, which are showing macroscopic quantum effects in quite a natural way, promote the coherence of quantum states, and so the attention of quantum computing community has been focused on superconducting and superfluid systems [5]. The idea of Josephson junctions as the principal building block of qubits was proposed by [6], and its compact mathematical description can be found in [7]. Indeed, such quantum computers can be realized on ion trap systems or on superconducting circuits [8], [9].

However, the Josephson junction suffers from fundamental scaling limitations since its dimensions are limited by the superconducting coherence length that is a measure of the Cooper pair size. For conventional, low-temperature superconductors, such as Nb, it is usually in the range of few thousand angstroms, thus, two orders of magnitude greater than the channel length in current CMOS transistors. Furthermore, the system cost of ion traps or Josephson junctions is inherently very high due to the need of cooling the whole structure down to, for example, ∼15 mK.

On the other hand, the past few decades have witnessed the unprecedented progress in the scaling of CMOS transistors down to several nanometers. This aggressive miniaturization has brought along a number of challenges, but also some interesting solutions. New materials and properties, innovative architectures and designs require sophisticated tools for the simulation and analysis of these structures [10]–[12]. As they are reaching atomic dimensions, quantum phenomena should now be taken into consideration.

The associate editor coordinating the review of this manuscript and approving it for publication was Marcello Caleffi.

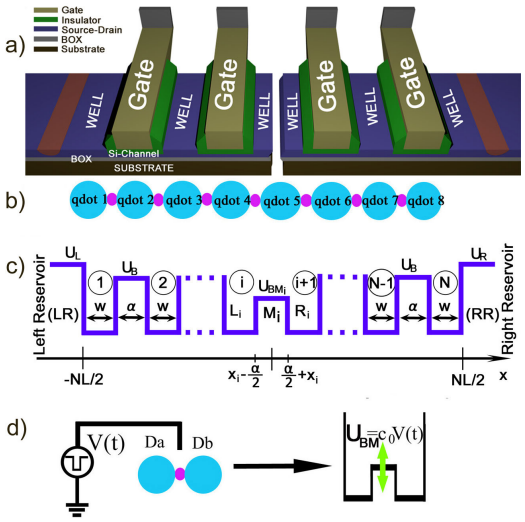

FIGURE 1. **(a) Series of CCD-like devices which form an electrostatically controlled qubit structure of 8 quantum wells/dots. (b) Equivalent quantum dot representation. (c) Eight-potential well structure with U_L and U_R denoting the height of the potential function at the left and right edges, respectively, and U_{BMi} denoting the height of the middle barrier. The total length is NL, where N is the number of wells. The length of the barrier is a and the length of each well is w. (d) Schematic representation of two neighbor dots, D_a and D_b, with electron transfer between them. One can manipulate the height of the potential barrier between the wells by applying a voltage pulse, $V(t)$, facilitating occupancy oscillations of quantum state. (U_{BM} is the barrier height and c_0 is a constant.).**

We surmise that operating qubits at the 4 K temperature of liquid helium would bring the total cost down significantly. There are active discussions regarding the realization of qubits that are compatible with CMOS and cryo-CMOS technologies [13]. Such qubits fabricated in silicon can be realized using electrostatically controlled quantum dots of various geometries [14], [15]. Electron transport can be achieved by employing a structure similar to that of charge-coupled devices (CCD), as shown in Fig. 1(a) [12]. A quantum-well-based coupled single-electron spin-qubit was studied in [16]. Recently, new approaches to Si/SiGe-based qubits were also proposed by various groups [17]–[20]. Other CMOS compatible realizations of qubits may be inspired by single-electron devices [21]–[23]. The behavior of single electrons in various nanostructures can be spotted using atomic force microscope [17] which has its importance for the development of single electron devices. Furthermore, the purity of silicon crystalline structure (as well as interface between the silicon and silicon-dioxide) has been constantly improving over the past decades to the point that it is now just below the level of military-grade plutonium. This is dictated by the need of being able to reliably manufacture billions of nanometer-size transistors on a single silicon die. In addition, the recent developments in Fully Depleted Silicon-on-Insulator (FD-SoI) and FinFET technologies further isolate the MOS device structures from the silicon substrate. This should improve decoherence and dephasing of MOS-based qubits. As a final point on CMOS qubits: Even though the decoherence time might still be shorter here than with the currently leading approaches, the CMOS quantum gates could compensate it with expected delays of orders-of-magnitude shorter due to the superior performance of nanometer-scale CMOS technology (e.g. cut-off frequency, f_T, in 16-nm FinFET is 750 GHz).

The functionality of classic voltage-controlled gates and their operation, when implemented as quantum gates, need to be studied both in the framework of electrical circuit engineering and in the framework of time-dependent modeling of quantum state dynamics. It requires the development of theoretical models of charge-induced CMOS quantum dots behaving like single-electron transistors, as well as the development of effective cryogenic models of CMOS circuits combined with experimental confirmation of predicted operation modes [13].

In this work, we discuss realistic aspects when constructing electrostatic qubits that are based on electron position in a multiple-dot system. The proposed scheme can change the quantum computing hardware paradigm as it moves away from the conventional spin-based qubits that must be cooled down to 15 mK. It utilizes a nanoscale CMOS technology at temperatures in a range of 4 kelvins [13]. At these temperatures, most charge carriers in semiconductors are frozen, but it is possible to maintain the functionality of CMOS devices by inducing a quantum state inside quantum wells formed by metallic gates operating under certain DC and AC voltages. The presented research is expected to have its importance in the construction of non-spin based quantum computers or hybrid semiconductor classical-quantum computers. The latter appears to have high potential of being commercially implemented in the near future.

The paper is organized as follows. Section II summarizes state-of-the-art in quantum technology and qubits. In Section III, we start presentation of the problem with a Schrödinger formalism, providing an insight into the physics of the system and giving tools to capture the most general characteristics from first principles. Leveraging the fact that the Schrödinger equation has an analytical solution in the approximation of a piece-wise potential, we provide a methodology to solve this problem by an example of an eight-well system. As a further development of the problem, we also provide a tight-binding methodology for the same system as an alternative to the Schrödinger formalism. In Section IV, we present the main results in the behavior of a semiconductor qubit obtained by employing the methodology of Section III. We draw conclusions on qualitative behavior, such as occupancy oscillations, delocalization and dephasing. In Section V, as one of the developments of this work, we derive a time-dependent semi-analytical numerical scheme, which allows one to capture the dynamics in the case of a time-dependent Hamiltonian. Purely numerical schemes are well developed for the time-dependent Schrödinger equation [24], [25]. In the proposed scheme, however, the evolution of the system in time is described in terms of the probability amplitudes of contributing quantum states, which are determined numerically, whilst the spatial eigen-functions

are determined analytically for each time step. This provides the advantage of tracking the system dynamics by knowing its eigen-functions at each time instance under the adiabatic assumption [26].

As a very illustrative example of this semi-analytical technique, we present in Section VI.A a case of a weak electrostatic interaction between two electrons confined in separate potential wells. In such a picture, their interaction can be seen as a perturbation to the initial dynamics of two electrons. This allows us to demonstrate a first signature of quantum correlation in electrostatically interacting quantum systems after a strong quantum measurement is applied to one of the particles. The same system is also studied with a non-pertubative tight-binding method in Section VI.B. We show that the proposed scheme gives qualitatively the same results. However, it includes entangled states in a straightforward way and it can be expanded to many-particle problems and larger systems of such structures. Comparing both approaches, we note that although one of the greatest advantages of the Schrödinger formalism is the ability to capture spatial properties of the wave-function, as the system grows large and its complexity increases, the Schrödinger formalism becomes computationally expensive in the case of many-body interaction. The introduced tight-binding approach, while not capable of providing some details, allows for an effective numerical implementation and can easily accommodate the electron interaction as well as some many-body phenomena.

II. STATE-OF-THE-ART OF QUANTUM TECHNOLOGY AND QUBITS

Quantum mechanics introduces the superposition of states and massive parallelism together with non-local correlations that are all absent in the classical physics [27], [28]. However, these phenomena occur only at a time scale that is limited by decoherence times (T_1 and T_2 in [29]). Decoherence processes are naturally incorporated in non-equilibrium Green functions as pointed out in [30]. In addition, the desired quantum phenomena can be sustained only under specific thermodynamic conditions and only for certain confining potentials. Therefore, on one hand, a quantum system intended to implement a qubit needs to be maximally decoupled from the outside world in order to keep its unique quantum features, such as quantum coherence. On the other hand, an observer must be able to interact with the quantum system, which brings the need for a ''not-so-small'' interaction between the qubit and a classical or semi-classical interface.

All the existing qubits impose certain trade-offs between their technical parameters and their ease of implementation and further scalability. A first option is to choose a system which is maximally decoupled from the external world. Trapped ions are seen as such systems since they are confined and suspended in free space using strong magnetic and electric fields. Observations of a relatively large number of entangle trapped ion qubits have been already made [31]. As indicated by many experimentalists, it impossible at this stage of technology to implement complicated topologies of electromagnetic confinement fields that would be 'stable'. For this reason, there are a limited number of trapped ion configurations, with the most common configuration being an in-line arrangement. The decoherence time of trapped ions is more than promising, within a range of seconds, which makes it four orders of magnitude greater than the decoherance time provided by any other quantum technology available so far. Just as other quantum processors, trapped-ion quantum processors [32] need to be cooled down to extremely low temperatures. Since the trapped ions can be arranged in a limited number of stable configurations, it is difficult to miniaturize them or scale them up.

TABLE 1. Quantum technology in various physical systems.

Q-Technology	Scalability	Time T_1	Time T_2
Ion traps [S]	Low	10^{10} μs!	10^{6} μs!
Semiconductor qubits			
(quantum dots):	High	1 ns-10 μs	1 ns-40 μs
1: [C]harge qubit	High	7 ns	250 ps
2: [S]pin qubit	High	$>$ 40 μs	40 μs
3: [S]pin singlet-triplet	High	$>$ 10 μs	10 μs
4: [S]pin exchange	High	$>$ 19 ns	19 ns
5: [S]resonant exchange	High	$>$ 16 ns	16 ns
6: [S]pin-[C]harge	High		80 ns
Superconducting qubits			
(Josephson junctions):	Medium	0.1-100 μs	0.1-100 μs
7: Cooper pair box [C]	Medium	2 μs	2 μs
8: Flux qubit [S]	Medium	4.6 μs	1.2 μs
9: Phase qubit	Medium	0.5 μs	0.3 μs
10: 3DTransmon[SC]	High	$>$ 100 μs	$>$ 140 μs
11: 2DTransmon[SC]	Medium	50 μs	20 μs
12: Fluxm [SC]	Medium	1000 μs	$>$ 10 μs
13: C-shunt [SC]	Medium	55 μs	40 μs
14: Xmon [SC]	Medium	50 μs	20 μs
15: Gatemon [SC]	Medium	5.3 μs	3.7 μs

The construction of qubits and quantum gates can be based on two-spin states of an electron or two-polarization states of a photon [27], [28]. Moreover, in addition to solid-state or superconducting spin qubits [S in Table 1] [33], [34], the position of an electron itself can be seen as a candidate for a qubit implementation. In this case, one can use solid-state devices and structures to manipulate them. For instance, the presence or absence of an electron in a quantum dot can be seen as the two states of a qubit. Such systems are known as charge (electrostatic) qubits [C in Table 1]. In particular, the semiconductor implementation of a charge qubit can be achieved through a single electron device [35]–[38]. In superconductor, one can use a Cooper pair box [40], [41] that has some features of the semiconductor position-based qubit as it is also controlled by electric field and relies on charge quantization. However, the electron-electron interaction is quite strong in comparison with the spin-spin interaction. For this reason, it is observed that charge qubits have a shorter decoherence time (since it is inversely proportional to the strength of interaction) and it has motivated the most of scientific community to move towards spin-based qubits.

Quite recently, steady progress has been shown in superconducting technologies where the decoherence time is

increasing, as pointed out by IBM Q-Experience or by Google. Fundamental modeling of decoherence processes can be achieved with the use of non-equilibrium Green functions [42], [43] and Keldysh contour, but it is only possible when one knows the exact Hamiltonian terms involved in the decoherence processes. In the case of superconductors, a flux qubit is controlled by a magnetic field (similarly to the spin-based qubit), or a Cooper pair box, which is a charge qubit, is controlled by an electric field. A compact mathematical description of basic superconducting qubits can be found in a phenomenological picture drawn by Nori [43] or in a more microscopic and mathematically compact picture in [7].

So far, the most successful quantum technology in terms of the decoherence time (excluding the ion traps which suffer from limited feasibility) is a combination of spin technologies and electron charge (see [S] and [C] references in Table 1). However, it is observed that spin-based qubits proposed in [16], [45] have a longer decoherence time than charge-based qubits [C]. This is, again, due to the fact that the electron-electron interaction cannot be screened out at short distances and is stronger than the spin-spin interaction, thus resulting in shorter decoherance times for charge qubits. To mitigate this, the use of hybrid spin-charge superconducting qubits, e.g. transmons, was proposed to suppress the 1/f noise as one of the main causes of decoherence[46]. A review of superconducting technologies can be found in[47], and a description of recent semiconductor technologies is given in[48].

The details on current quantum technologies are given in Table 1 which presents currently used semiconducting and superconducting qubits, as well as ion traps.

III. MATHEMATICAL STATEMENT OF THE PROBLEM

A. PRELIMINARY VIEW

The system under study consists of multiple quantum wells (acting as quantum dots) in which an electron can transition between two neighboring wells. The structure can be directly implemented in CMOS [2] and, especially now, in nanometer-scale CMOS with options to further isolate the devices through an insulating layer (e.g. FD-SoI) or by raising them (e.g. FinFET). When all the wells are arranged in series, they form an array similar to a CCD. A charge carrier (an electron or hole) can flow between two neighboring wells, which are controlled by applying a voltage waveform $V(t)$ that would lower or increase the gate bias at specific times. A representative visualization of such a geometry is shown in Fig. 1(a), and the corresponding quantum dot representation is shown in Fig. 1(b). Figure 1(c) depicts an equivalent model of the potential arrangement for this system, which can be considered as a series of piece-wise potential wells that might have discrete translation symmetry as in an atomic crystal lattice. In this paper, we will first focus on the state development of one electron, which can tunnel between any two selected potential wells, L (left) and R (right), in an eight-well system. In this picture, a quantum well can trap a single electron. An imposer (e.g., a CMOS gate) is placed between the two wells, enabling the manipulation of the height U_{BM} of the corresponding potential wall that separates the two wells L and R, as shown in Fig. 1(d).

By applying a voltage pulse at the separating wall, one can lower the barrier between the wells to initiate quantum tunneling. In this case, the electron displays occupancy oscillations (known in the literature as Rabi oscillations in the case of a time-dependent Hamiltonian [48]). The maximum amplitude of oscillations will be achieved when the frequency of the external driving field matches the frequency of tunneling, ω_0. In a simplified approach, for the time period when the potential remains constant, the electron quantum state $|\psi\rangle$ can be represented as the solution of the one-dimentional (1D) time-independent Schrödinger equation for a piece-wise square-well potential. Furthermore, the full time-dependent wave-function $|\Psi|^2$ oscillates with a frequency ω_0, which is determined by the applied voltage, the geometry of the structure and the properties of the material. It should be noted that possible fluctuations of the potential barriers (both fast and slowly varying), in the most general case of a time-dependent Hamiltonian, can alter the Rabi frequency. The dependence of ω_0 on the imposer voltage will be shown to be exponential, and, therefore, very sensitive to minute variations of its value. It should also be noted that a key element in the performance of quantum dots is decoherence time since the stability of state superposition is an essential requirement for quantum operations. Environmental coupling is the major factor, albeit not the only one that affects the decoherence. The isolation of such a system, operation at cryogenic temperatures, and small dimensions of the devices (smaller transistors are expected to interact less with the environment) must all be embraced.

In this work, we perform a direct calculation of ω_0 for an electrostatic structure of a particular geometry. In such a scenario, $|\psi\rangle$ can be expressed as a superposition of two states, which can be denoted as $|0\rangle$ and $|1\rangle$. Such a quantum bit is based on the electron's position, i.e., in a two-well system $|0\rangle$ can denote the state where the electron is localized in the left well, and $|1\rangle$ when it is localized in the right well.

B. SELECTION AND JUSTIFICATION OF THE MODEL

1) AIM OF MODELLING

Using the model presented in this section, we aim to achieve the understanding of the system from *first principles*. Hence, we start the model development from the Schrödinger formalism. This model is not intended for precise simulations, but rather for capturing the most significant and important physical phenomena.

For all simulations in this paper, unless stated otherwise, we will use parameters presented in Table 2. We use either a two-well case (mostly as an illustrative example) or an eight-well case (as an example of a realistic coupled-dot structure).

TABLE 2. Parameters used in simulations.

Length of device	L	200nm
Barrier width	a	0.25 L
Width of device	d	0.4 L
Middle barrier height	U_{BM} (double-well system)	120 E_0
Middle barrier height	U_{BM} (eight-well system)	200 E_0
Left/right barrier height	$U_L = U_R$	400 E_0
Tight binding energy	$E_{p1} = E_{p2}$	9.37 E_0
Tight binding hopping	ts	0.23 E_0

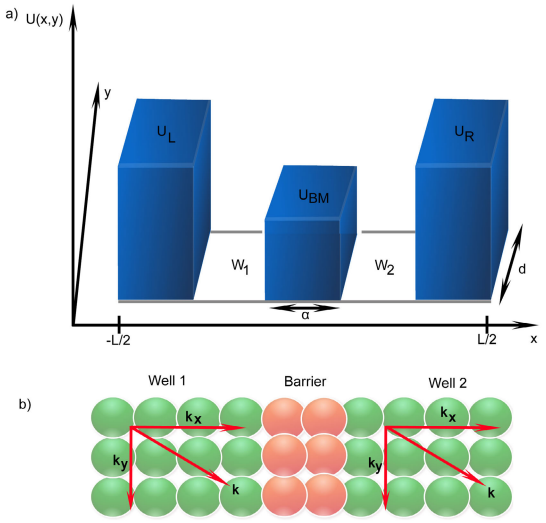

FIGURE 2. 2D view of the two-well structure: (a) double-well potential in the (x, y) plane and (b) 2D equivalent lattice.

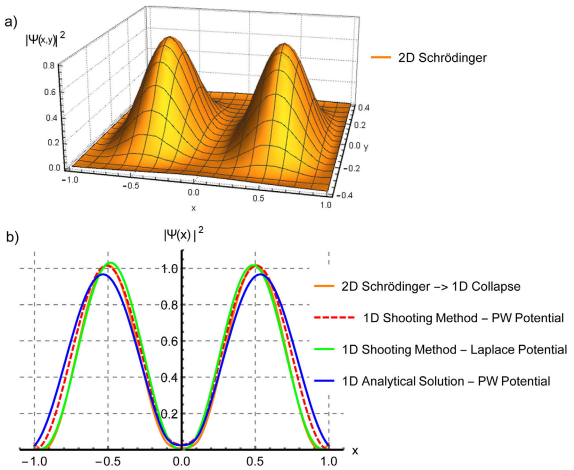

FIGURE 3. (a) Probability density $|\psi(x, y)|^2$ of the ground state from the numerical solution to the 2D Schrödinger equation with a two-well piece-wise potential. (b) Comparison of the probability density $|\psi(x)|^2$ of the ground state calculated from four different models: 2D Schrödinger equation with the reduction to the x-dimension (orange line), 1D Schrödinger equation with a piece-wise potential using a shooting method (dashed red line), 1D Schrödinger equation with a smooth potential using a shooting method (green line) and analytical solution to the 1D Schrödinger equation with a piece-wise potential (blue line).

2) FROM 2D TO 1D MODELLING: JUSTIFICATION OF MODEL REDUCTION

We begin by justifying our choice of the 1D Schrödinger formalism. In this section, we show that the presented formalism can capture the major physical effects in a correct fashion.

Due to the geometry of the system, see Fig. 1, where two dimensions (length and width) dominate over the third dimension (depth), one may consider to use the 2D Schrödinger equation. The 2D potential function to be used is shown in Fig. 2(a). The wave-function $|\psi(x, y)\rangle$ of an electron injected into such a potential is subject to the 2D steady-state equation:

$$\hat{H}\,|\psi\rangle = \hat{E}\,|\psi\rangle \tag{1}$$

where $\hat{H} = \frac{\hat{p}^2}{2\,m_e^*} + U(x, y)$ is the Hamiltonian operator, which is the sum of kinetic and potential energies, $U(x, y)$ is the potential energy, $\hat{p} = -i\hbar(\frac{\partial}{\partial x} + \frac{\partial}{\partial y})$ is the momentum operator, m_e^* is the effective electronic mass and $\hat{E}$ is the matrix with eigen-energies of the system.

When solving such an equation, the system can be represented as a 2D lattice of unit cells interconnected by bonds (see Fig. 2(b)) where k, k_x and k_y denote the directional wave-numbers). As long as the structure can be assumed uniformly periodic in the x-direction, and by assuming that the length of the structure L is significantly longer than the width d (i.e., the structure can be approximated by a 1D wire, which is the case as the number of potential wells in series increases), the eigen-function in the y-direction can be expressed in the form of plane waves [49], [50]. This is clearly visible from the numerical solution to the 2D Schrödinger equation shown in Fig. 3(a). (Many schemes can be used to solve such an equation numerically, e.g. the relaxation variational numerical method [51], the shooting method [52], etc.). We also pre-impose a symmetry of the system in y-direction (i.e. a periodic behavior of $U(y)$), e.g. by assuming the occurrence of a large number of parallel strips, as depicted in Fig.2. Looking from an another analysis perspective and by assuming a small variation of $\psi(x, y)$ across the nanowire, one can make a transition from the 2D wave-function $\psi(x, y)$ to its effective reduced 1D version by applying an integration with respect to the y-dimension:

$$\psi(x) = A \int_d \psi(x, y)dy \tag{2}$$

where A is a normalization coefficient and d is the width of the device.

Another insight into a possible reduction of the system with respect to the y-dimension can be provided by solving the transmission problem with use of the probabilistic current:

$$J(r, t) = \frac{i\hbar}{2m_e^*}[\psi(r, t)\nabla\psi^*(r, t) - \psi^*(r, t)\nabla\psi(r, t)] \tag{3}$$

In our case, the transfer of electron occurs strictly along the x-axis, so we are interested only in the J_x component of the current. As one injects an electron into the first well of

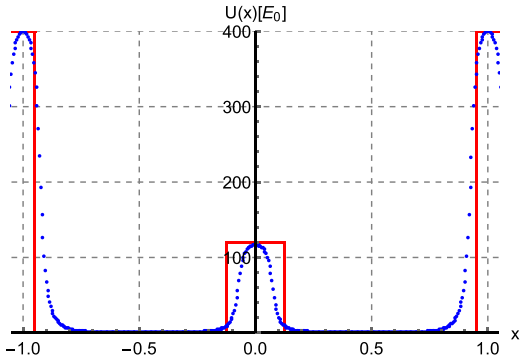

FIGURE 4. Example of an effective electric potential profile between two wells calculated with Laplace equation (blue line) and its square piece-wise approximation (red line).

the chain, a single-electron detector "catches" it at the end of the chain during the measurement after the electron is controllably transferred along x-spatial dimension [53].

Figure 3(b) compares the wave-function $\psi(x)$ of the ground state in the x-direction obtained from four different models: numerical solution to the 2D Schrödinger equation projected onto the x-direction (2), 1D Schrödinger equation with a piece-wise potential solved using a numerical technique, 1D Schrödinger equation with a smooth potential solved using a numerical technique, and 1D Schrödinger equation with a piece-wise potential solved using an analytical method. The most important conclusion we draw from this comparison is that in case of the thin semiconductor nanowire neither the reduction from 2D to 1D nor approximating the potential by a piece-wise function will result in a significant error. Again, since we are interested in the electron transfer along the x-axis, we conclude that the use of the 1D model with a piece-wise potential is justified.

3) FROM SMOOTH TO PIECE-WISE POTENTIAL FUNCTION: JUSTIFICATION OF POTENTIAL FUNCTION CHOICE

At this stage it is also useful to briefly discuss the piece-wise approximation for the potential function. This approximation implies that instead of a smooth potential function seen by an electron in such a structure, we use its piece-wise simplification shown in Fig. 4.

We remind the reader that Fig. 3(b) shows the probability density $|\Psi(x)|^2$ of the ground state for the four models discussed in the previous subsection, with two of them utilizing the piece-wise potential approximation. This approximation does not pose any noticeable issues or solution inaccuracies.

Yet, there is a significant benefit in using the piece-wise potential function in the Schrödinger equation. It allows one to obtain analytical solutions to the equation. Additionally, in such a case, we know precisely the shape of wave-functions $|\psi(x)\rangle$, i.e. their space distribution. Moreover, we must obtain and incorporate them in a time-dependant numerical scheme which will provide their evolution in time (as will be done in a later section).

C. COUPLED QUANTUM DOTS IN THE SCHRÖDINGER FORMALISM

Having justified the benefits and applicability of the 1D Schrödinger equation, we shall now use it to show the electron's behavior and transport in a system of N quantum wells. We note that for specific numerical simulations presented in later sections, we take $N = 8$.

The system of N wells can be represented by a double square-well potential (DWP) of total length NL, as shown in Fig. 1(c), where a is the individual barrier width and U_L, U_R and U_{BM_i} are the barrier heights for the left, right and middle barriers, respectively.

By introducing the dimensionless position $\xi = x/L$ and a new unit of energy $E_0 = \frac{\hbar^2}{m_e^* L^2}$ (which has the meaning of the ground energy in an infinite potential well of length L), one can write equation (1) in a dimensionless form:

$$-\frac{\partial^2}{\partial \xi^2}\psi(\xi) + [U(\xi) - E]\psi(\xi) = 0 \tag{4}$$

Studying the case of eight wells, the potential function spans the space over the range $\xi \in [-4, 4]$, and the system is symmetrical with respect to the origin (assuming $x_i = 0$ for the middle barrier).

While it is pedagogical to assume that $U_L = U_R = \infty$ for simplicity [54], here we will not consider infinite barriers at the edges, assuming, therefore, $U_L, U_R \neq \infty$. This will allow us to account for various configurations that can occur in the considered quantum dot structure. The wave-function for large potential barriers is expected to decay exponentially in the classically forbidden regions at $|\xi| > N/2$. However, as one gradually lowers the barriers, the probability for an electron to escape the potential well increases. We denote this probability as the "leakage" (δ_{LK}) of the wave-function. This "leakage" can potentially have a significant impact on the performance of the system under study. For the system of Fig. 1(d), $U(\xi)$ is a piece-wise function:

$$U(\xi) = \begin{cases} U_L & \xi \leq -N/2 \\ 0 & -N/2 < \xi < -N/2 + w \\ \vdots & \\ U_{BM_i} & -a/2 \leq \xi \leq a/2 \\ 0 & a/2 < \xi < a/2 + w \\ \vdots & \\ U_R & \xi \geq N/2 \end{cases}$$

D. TOWARDS THE DESCRIPTION OF COUPLED QUANTUM DOTS AND INTERACTING ELECTRONS IN THE TIGHT-BINDING FORMALISM

One great advantage of the Schrödinger formalism is that it captures the spatial distribution of the wave-function and its geometrical dependencies for a given system from first principles. However, it is not optimal for many-particle systems since it is computationally expensive.

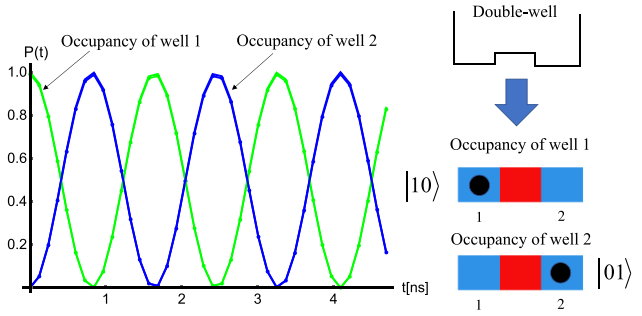

FIGURE 5. Occupancy evolution in a double-well system constructed with the Schrödinger formalism (dots) in comparison to tight-binding formalisms (lines). The two methodologies are equivalent.

For structures with interacting electrons, or in the most general case many interacting particles, a tight-binding formalism shall be proposed [55], [56]. At the core of this approach is the assumption that each particle, while interacting with others, stays confined to its own potential. Our ultimate goal is to introduce the tight-binding formalism for multiplicity of interacting electrons bound to their two-well potentials.

In this section, we begin with a simplified problem and show how to treat one electron in a two-well potential in the tight-binding formalism. Later on, we will expand it to describe the two-body interaction with a non-pertubative approach. We shall highlight here that we consider a two-well system as an illustrative example. In the tight-binding formalism, the original two-well system is seen as a *two-state system*, as shown in Fig. 5. As defined before, the state $|10\rangle$ corresponds to the localization of an electron in well 1 (with well 2 being empty), and $|01\rangle$ corresponds to the localization of an electron in well 2 (with well 1 being empty).

The Hamiltonian of such a system can be written as:

$$H = \begin{bmatrix} E_{p_1} & t_{s,1\to 2} \\ t_{s,2\to 1} & E_{p_2} \end{bmatrix} \tag{5}$$

where t_s is the tunneling (hopping) term between the two states and E_p is the potential energy. In such a notation, the wave-function can be expressed as a superposition of the two states:

$$|\psi\rangle = a\,|10\rangle + b\,|01\rangle \tag{6}$$

where $a(t)$ and $b(t)$ are the occupancy coefficients in the Wannier-position basis $\{|10\rangle,|01\rangle\}$.

Utilizing the tight-binding formalism with the piece-wise potential function introduced in this section and the tunneling rate between the two states, we plot in solid lines in Fig. 5 the occupancy of states $|10\rangle$ and $|01\rangle$ over time. For comparison, we indicate in dots the occupancy oscillations obtained from the 1D Schrödinger formalism. We observe the classic occupancy (Rabi) oscillations, which are typical for two-state quantum systems. We also note that these oscillations are identical in both (i.e. Schrödinger and tight-binding) formalisms, which shows the validity of tight-binding formalism in the context of position-based qubits.

IV. ELECTRON TRANSFER AND OCCUPANCY OSCILLATIONS FROM THE SCHRÖDINGER EQUATION

A. METHODOLOGY OF SOLUTION

Equation (4) can be written as $\frac{d^2}{d\xi^2}\psi - \beta^2\psi = 0$, with $\beta = \sqrt{U(\xi) - E}$. The general form of the solution to such a second-order differential equation is a family of plane waves:

$$\psi(\xi) = c_0^r \exp(ik\xi) + c_1^r \exp(-ik\xi) \tag{7}$$

where c^r are constants (the superscript r denotes different regions of the piece-wise well profile) and $k = 2\pi/\lambda$ is the wave-number. The wave-function is subject to the boundary conditions $\xi \to \pm\infty,\ \psi(\xi) \to 0$, or

$$\begin{aligned} \xi < L, \quad & c_1^{LR} = 0,\ \psi_{LR}(\xi) = c_0^r \exp(k\xi) \\ \xi > L, \quad & c_0^{RR} = 0,\ \psi_{RR}(\xi) = c_1^r \exp(-k\xi) \end{aligned} \tag{8}$$

where the sub-index in the wave-function denotes the corresponding region of the potential well: e.g., ψ_{LR} is the wave-function in the LR region of Fig. 1(d). In addition, the solutions in the regions L_i and R_i can be simply written as a superposition of sinusoidal functions since we assumed $U = 0$ there:

$$\psi_{L_i,R_i}(\xi) = c_0^{L_i,R_i} \cos(\beta\xi) + c_1^{L_i,R_i} \sin(\beta\xi) \tag{9}$$

The continuity conditions on the wave-function $\psi(x)$ and its first derivative determine the coefficients c_k^r. For each boundary of N-potential well, one can write two continuity equations:

$$\begin{aligned} \xi = -N/2: \ & \psi_{LR} = \psi_{L1},\ \frac{d}{d\xi}\psi_{LR} = \frac{d}{d\xi}\psi_{L1} \\ & \vdots \\ \xi = -\alpha/2: \ & \psi_{L_i} = \psi_{M_i},\ \frac{d}{d\xi}\psi_{L_i} = \frac{d}{d\xi}\psi_{M_i} \\ \xi = \alpha/2: \ & \psi_{M_i} = \psi_{R_i},\ \frac{d}{d\xi}\psi_{M_i} = \frac{d}{d\xi}\psi_{R_i} \\ & \vdots \\ \xi = N/2: \ & \psi_{R_N} = \psi_{RR},\ \frac{d}{d\xi}\psi_{R_N} = \frac{d}{d\xi}\psi_{RR} \end{aligned} \tag{10}$$

By rearranging the system of equations (10) into canonical form $\mathbf{A}\xi = 0$, where $\mathbf{A}$ is the matrix of coefficients c_k^r, we demand $\mathrm{Det}(\mathbf{A}) = 0$ for the system to have non-trivial solutions. The latter equation gives us the (normalized) eigen-energies ϵ_j of the Hamiltonian operator. Then, with known ϵ_j, the coefficients c_k^r can be calculated by solving the system (10) of continuity equations, including the normalization restriction for the coefficients of each wave-function, i.e., $\sum_k |c_k^r|^2 = 1$. Due to technicalities, exact solutions of Schrödinger equation for a finite many-well system (as, for example, for the eight rectangular wells here) are usually omitted in the literature but are presented in this work due to their importance for the implementation of interacting quantum dots. As it will be discussed and demonstrated later, an analytical solution can allow one to determine the intrinsic features of a given geometry, and more specifically,

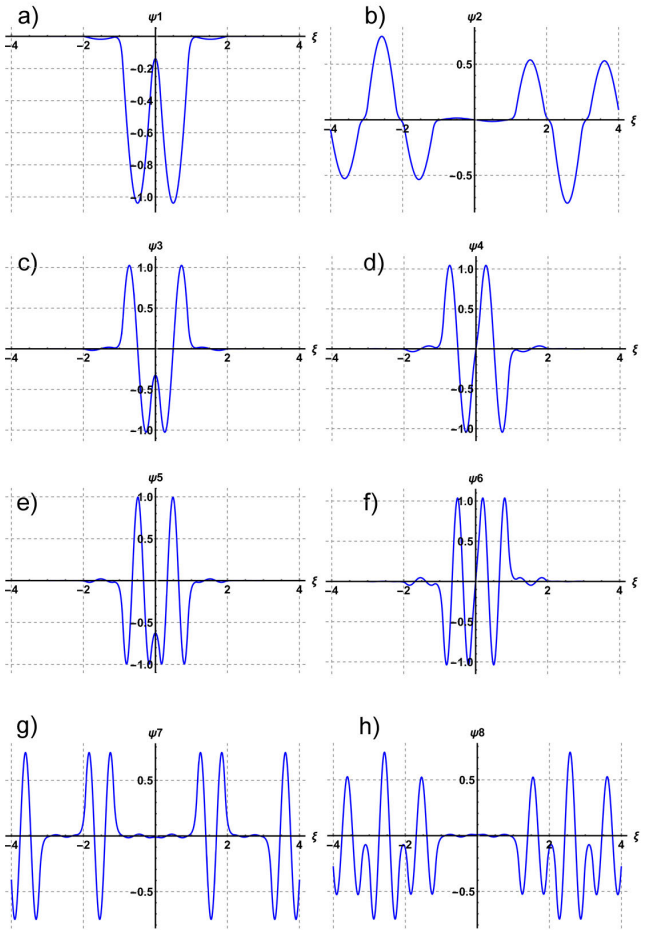

FIGURE 6. Eigen-functions of an eight-well system for the first eight energy levels: (a) even solution, and (b) odd solution for the first energy level split; (c)–(d) are those of the second energy level split; (e)–(f) and (g)–(h) are those of for the third and fourth energy level splits, respectively.

to explicitly calculate the "leakage" of the wave-function (i.e., the presence of wave-function solutions in classically forbidden regions). The determination of the latter property will be used later in modeling the delocalization of a quantum state confined in such structures.

For each energy level ϵ_j, there is a corresponding eigen-function $\psi_j(\xi)$, and their set gives us the state $|\psi\rangle$. Any superposition of these functions $\mathbf{c}^0 |\psi\rangle$ (where $\mathbf{c}^0$ is a row vector of constants obeying the normalization rule) also gives a quantum state. The time-dependent function can then be expressed as follows:

$$\Psi(\xi, \tau) = e^{-i\epsilon_j \tau} c_j^0 \psi_j \tag{11}$$

where the repeating index implies summation. In Fig. 6, we plot the eigen-functions for the first eight energy levels in an eight-well system, where we have assumed a lowered barrier in the middle of the structure. Notice that for this geometry the ground state is a symmetrical solution, whilst the first excited state is an anti-symmetrical solution (this property is denoted often as "parity"). These two first solutions have nearly identical wavelengths

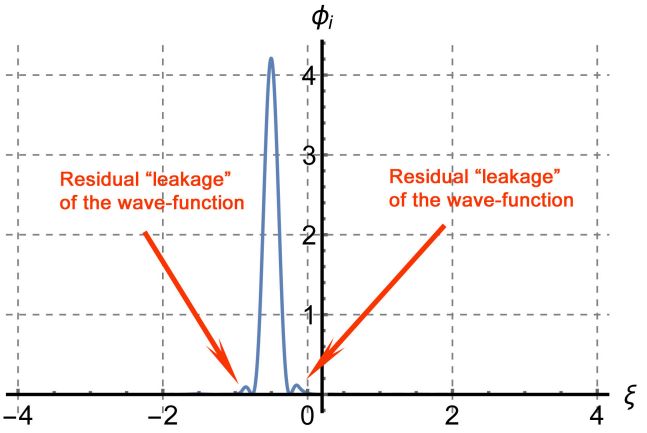

FIGURE 7. Example of a maximally localized wave-function for the system of eight coupled wells that can be obtained with the use of a linear transformation.

and therefore close (but not equal) energies. This is due to the fact that in the 1D case, the degeneracy of energy is not possible [57], [58]. In the same manner, each symmetrical eigen-function, which corresponds to a given eigen-energy, comes with an anti-symmetrical one with a slightly higher eigen-energy. Depending on the available energy of the electron, more eigen-energies and eigen-functions can be involved in the state's superposition, with the number of bound eigen-energies for the system being determined from the Bargmann's theorem [59].

We note that the set of eigen-functions $|\psi\rangle$ does not correspond to localized states of an electron injected in such a structure. However, their superposition can indicate the electron's location. To show that a localized state can be constructed using the eigen-functions, we apply the unitary transformation $\mathbf{\Gamma}$:

$$|\phi\rangle = \mathbf{\Gamma}^T |\psi\rangle \tag{12}$$

which gives a set of normalized orthogonal functions $|\phi\rangle = \phi_j$ representing localized states. The transform Γ can be determined by solving a maximization problem, i.e., by maximizing $\int_w |\psi(x)|^2 \, dw$ in a given well. We note that $\langle \phi_i | \phi_j \rangle = \delta_{i,j}$. At this point, it is helpful to refer to a theory of maximally localized wave functions in systems with discrete translation symmetry that is known as Wannier function theory [60]. However, our methodology also covers the cases of perturbed potentials, systems with perturbed translation symmetry and systems with a lack of translation symmetry.

As we begin with the analysis of an isolated quantum system, its time evolution can be obtained by applying the unitary time evolution operator, $\hat{\mathcal{U}}$, to an initial state, $|\psi, t_0\rangle$ at time t_0. Then,

$$|\psi, t_0; t\rangle = \hat{\mathcal{U}} |\psi, t_0\rangle \tag{13}$$

or equivalently, in the $|\phi\rangle$ basis:

$$|\phi, t_0; t\rangle = \hat{\mathcal{U}} \Gamma^T |\psi, t_0\rangle = \Gamma^T \hat{\mathcal{U}} (\Gamma^T)^{-1} |\phi, t_0\rangle \tag{14}$$

In Fig. 7, the resulting localized function for the middle well (w_4) in an eight-well system is visualized. However,

we should mention that the localized states are not placed in the potential wells ideally, and the corresponding wave-functions are not vanishing immediately in the neighboring regions. Depending on a given geometry, the leakage of the wave-function into the classically forbidden region can be lager or smaller. Additionally, for some geometries, these localized functions might not be possible to construct with high accuracy. We will model delocalization processes in our system with the use of localized states that are due to the ''leakage'' of the wave-function, that is the presence of wave-function in classically forbidden regions, taking advantage of the Schrödinger formalism.

Finally, the frequency ω_O of occupancy oscillations between the n^{th} and m^{th} energy levels is given by the formula [61]:

$$\omega_O^{nm} = \frac{(E_n - E_m)}{\hbar} = \frac{\hbar(\epsilon_n - \epsilon_m)}{m_e^*} \tag{15}$$

B. MODELING DELOCALIZATION PROCESSES

One of the main issues related to the performance quality of quantum information processing systems is the property of information density scaling and qubit operational time [62]. Delocalization of the wave-function can result in a loss of information depending on the geometry of the structure at a given qubit implementation.

In this section, we visualize the delocalization phenomenon as a result of diffusion processes intrinsic in the Schrödinger equation. It can be partly represented as a ''leakage'' of the wave-function outside of the qubit region. Assuming a system of one electron performing oscillations of occupancy between M neighboring wells which define the qubit in a structure of N-wells (with $M < N$), we define the probability of finding the electron outside the M-wells at a given instance t_0 as $P_{\text{esc}}(t_0)$, and the probability of finding the electron inside the M wells as $P_{\text{ins}}(t_0)$. Then, the probability for the electron to be found inside the M wells after time t will be equal to the initial $P_{\text{ins}}(t_0)$ minus the accumulated probability of escaping $P_{\text{esc}}(t) = \int_{t0}^{t} \int_{\text{outside}} |\psi(x,\tau)|^2 \, dx d\tau$, with $P_{\text{ins}} + P_{\text{esc}} = 1$ at any time instance. Note that the probability for the electron to return is disregarded in this model. In Fig. 8, the delocalization simulated for an eight-well system is visualized where P_1 is the probability of the electron presence in w_4 and P_2 is the probability of the electron presence in w_5. We highlight though that such strong tendency to delocalization is due to the fact that we take into account up to eight lowest eigen-energies. For this reason, this is somewhat an extreme example shown to demonstrate the delocalization process.

C. MODELING DEPHASING PHENOMENA

Charge noise is the main effect of dephasing in quantum systems that are based on the manipulation of single electrons. In the simple case where the decay rate can be characterized by a unique relaxation time, dephasing can been seen as an exponential decay with time:

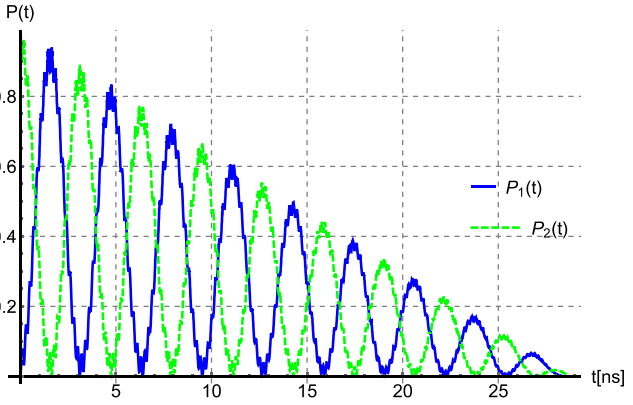

FIGURE 8. Delocalization visualized for an eight-well system.

$$\langle e^{i\phi_{nm}(t)} \rangle = e^{-\Gamma_{\phi_{nm}} t} = e^{-\frac{t}{T_2}} \tag{16}$$

where $\Gamma_{\phi_{nm}}$ is a ''dephasing'' rate and $\phi_{nm}(t) = -\frac{1}{\hbar}\int_0^t \epsilon(t')dt'$ is a fluctuating phase over the frequency ω_0^{nm} [63], [64]. In our system such a problem can arise when the potential profile, i.e. the effective potential field, is not constant but fluctuates with time. To control the qubit and perform quantum logic operations one has to apply valid voltage pulses which will allow to manipulate angles in a Bloch sphere. In such a case, the applied effective field can be treated as a controlled 'constant' component U_0 and a fluctuating component $u(t)$ which represents the noise [65].

In the Gaussian approximation, the phase $\phi_{nm}(t)$ accumulated by the stochastic quantity $u(t)$ is the sum of many uncorrelated contributions. Hence, for quantum dot devices which are dominated by low-frequency charge fluctuations, T_2 can be expressed as [37], [67]

$$T_2 = \pi S(0) \tag{17}$$

where $S(\omega)$ is the power spectrum of noise. By adopting the flicker noise model, and using an example of an FD-SoI device of [66], we obtain Fig. 9 for the geometry of our structure. From a practical perspective, with a qubit operational time on the order of tens of ps in this technology, several hundreds or even a thousand of operations could be realized within the window of decoherence time.

D. OCCUPANCY OSCILLATIONS AND THEIR FREQUENCY

Figure 10 presents a cycle of occupancy oscillations considering an eight-well system with a lowered barrier in the middle. Starting from a localized state in the left well (w_4) [see Fig. 10(a),(e)], the time-dependent wave-function $|\Psi(\xi,\tau)|^2$ oscillates between the fourth (w_4) and the fifth (w_5) wells. In Fig. 10(A1), four energy levels are considered. Figure 10(b) shows the electron's transition from the left to the right well. Figure 10(c) shows a state where the electron is localized in w_5. Finally, Fig. 10(d) shows a transition instance from the right to the left well. The corresponding probabilities

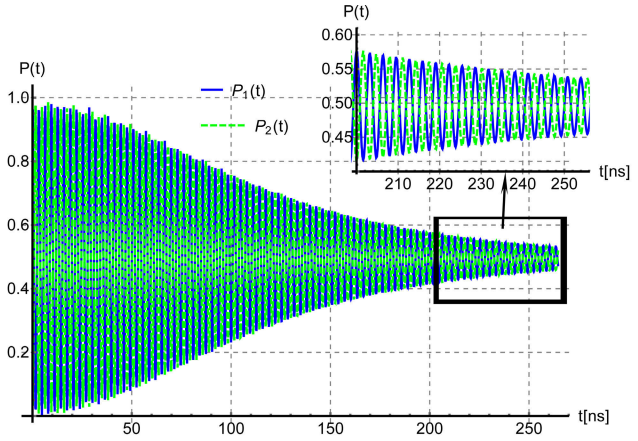

FIGURE 9. Dephasing evolution for a system of 8-wells for $1/f$ noise profile extracted from [66].

for the particle to be found in each of the two middle wells is given in Fig. 10(A2). An equivalent plot is also given considering the first *eight* eigen-energies [see Fig. 10(B1)]. As one considers more frequencies, the dynamics of the system become more complex. The overall behavior is periodic (as shown in snapshots (e)–(h) in that figure), and one can see that the probability of the wave-function is skewed. However, the transition between the two wells is still taking place [see Fig. 10(B2)]. We should note that there is always a small probability for an electron to escape to yet another well.

In principle, in the most general case, all the possible combinations for a given energy spectrum, or equivalently all the possible frequencies, can be found in the system transitions from one well to another. Figure 11(a) visualizes all the possible present frequencies in an eight-well system, considering the first eight eigen-energies. One can see that their values converge to a fixed discrete spectrum with an increasing gap as U_{BM} increases. However, in practice, not all of these frequencies will have the same impact on the dynamics of the system since the contribution of each eigen-function and eigen-energy to the construction of a localized wave-packet (which is the initial state that one assumes before beginning a given simulation) is of different magnitude. In particular, in this implementation, the two first energy levels are of greater significance. Figure 11(b) presents the calculated frequency $f_{O_{12}} = \omega_{O_{12}}/(2\pi)$ when only the two first eigen-energies (one for the symmetrical and one for the corresponding asymmetrical solutions) from expression (15) are drawn. One can see that there is an exponential dependence of the frequency on the height of the modified barrier U_{BM}. In an application featuring similar dimensions to these used in the simulations, where the electron operates in the first two energy levels, the oscillation of occupancy will be in the range of 5–20 GHz (line $f_{0_{12}}$).

We note that U_{BM} has a very strong impact on the electron transport between two quantum dots. Therefore, an accurate

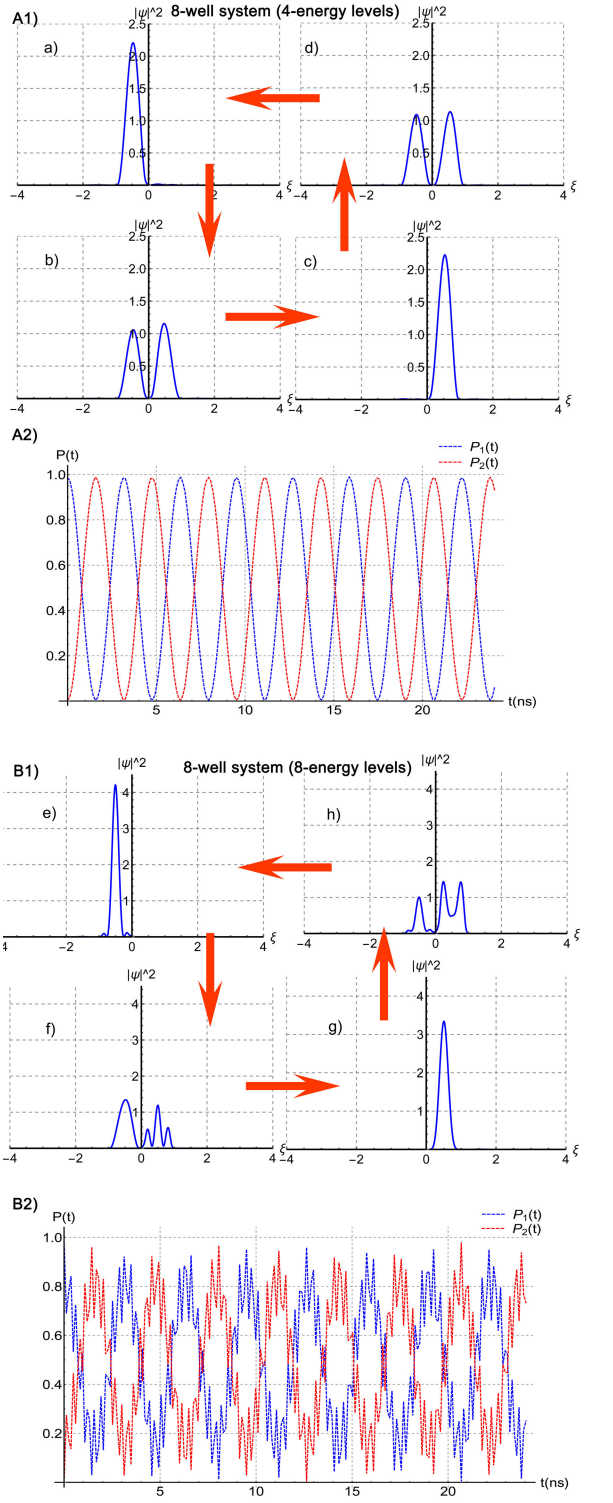

FIGURE 10. Occupancy oscillations in an eight-well system. (A1) only the first four energy levels are considered, with snapshots taken at four different instances of time: (a) electron is localized in the left well; (b) electron wave-function is distributed in both wells; (c) electron is localized in the right well; (d) electron wave-function is distributed in both wells again. (A2) Probability oscillations between the two middle wells; (B1) (e)-(h) the first eight energy levels are considered. (B2) Probability oscillations between the two middle wells.

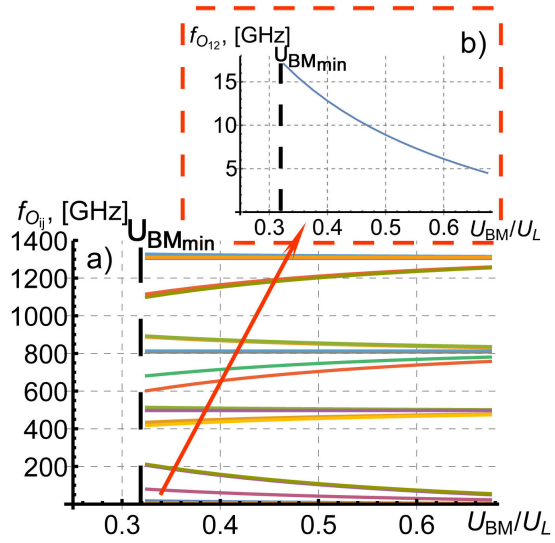

FIGURE 11. (a) Frequencies of occupancy oscillations $f_{O_{ij}}$ as a function of the height of the modified potential barrier U_{BM} in an eight-well system. The frequencies converge to a fixed discrete set with an increasing energy gap between them as U_{BM} increases. One can recognize the similarity of the obtained picture with the formation of energy band structures in solid-state crystals. It is the confirmation that the wells controlled electrostatically are indeed artificial atoms. (b) Frequency of occupancy oscillations $f_{O_{12}}$ between the two first energy levels as a function of the height of the modified middle potential barrier U_{BM} separating the two middle wells in an eight-well system. As expected, the frequency decreases exponentially with U_{BM}.

calculation of the frequency f_O is essential for the design and implementation of quantum dots. Additionally, the isolation of the system from the environment is of significant importance, since fluctuations of the surrounding environment might affect the quantum state occupancies and characteristic energy levels [68]. Moreover, it shall be noted that there are internal dynamics of noise coming from a thermodynamic ensemble, in which the quantum dots are placed. These dynamics are an inherent property of any physical system.

V. TIME-DEPENDENT PREDICTOR-CORRECTOR SEMI-ANALYTICAL NUMERICAL SCHEME

Let us describe a general time-dependent semi-analytical numerical scheme for the system, assuming an arbitrary number of bound states, k. The methodology can be expanded straightforwardly in the case of a continuous energy spectrum of the Hamiltonian. However, for the system under study, we are only interested in the bound states. We will use this scheme in the next section to analyze interaction between electrons.

Starting from the time-dependent Schrödinger equation:

$$i\hbar\frac{\partial\left|\psi(t)\right\rangle}{\partial t}=\hat{H}(t)\left|\psi(t)\right\rangle=E(t)\left|\psi(t)\right\rangle \tag{18}$$

one can write a discretized expression in time by using the first-order finite-difference approach:

$$\left|\psi\right\rangle^{n+1}=\left|\psi^n\right\rangle+\frac{-i\Delta t}{\hbar}\hat{H}^n\left|\psi^n\right\rangle=\left|\psi^n\right\rangle+\frac{-i\Delta t}{\hbar}\hat{E}^n\left|\psi^n\right\rangle \tag{19}$$

where n is the time index and $\hat{E}^n$ is the eigen-value matrix. The state of the system $|\psi\rangle$ at any time instance n can be written as:

$$\left|\psi^n\right\rangle=\sum_k c_k^n\left|\psi_k^n\right\rangle \tag{20}$$

where $\left|\psi_k^n\right\rangle$ are the eigen-functions of the Hamiltonian $\hat{H}^n$. The Hamiltonian can be expressed in a spectral representation as:

$$H^n=\sum_k E_k^n\left|\psi_k^n\right\rangle\left\langle\psi_k^n\right|, \tag{21}$$

where E_0^n, E_1^n, etc., are real-valued numbers and $\left|\psi_0^n\right\rangle\left\langle\psi_0^n\right|$, $\left|\psi_1^n\right\rangle\left\langle\psi_1^n\right|$ are the projectors for the corresponding Hamiltonian eigen-states. Then, plugging (20) and (21) into (19), while omitting the summation symbols, we get:

$$c_k^{n+1}\left|\psi_k\right\rangle^{n+1}=c_k^n\left|\psi_k^n\right\rangle(1+\Omega E_k^n) \tag{22}$$

where $\Omega=-i\Delta t/\hbar$. At any time instance n, the Hamiltonian H^n and the corresponding eigen-functions and eigen-energies can be calculated from the analytical methodology provided in Section IV-A. Therefore, one needs to calculate the evolution of coefficients c_k. By multiplying both sides of (22) by $\langle\psi_m|^{n+1}$ we get:

$$c_m^{n+1}=c_k^n\left\langle\psi_m^{n+1}\middle|\psi_k^n\right\rangle(1+\Omega E_k^n). \tag{23}$$

Notice, that the orthogonality of the eigen-functions applies only at the same time instance, i.e., $\left\langle\psi_m^n\middle|\psi_k^n\right\rangle=\delta_{m,k}$ but $\left\langle\psi_m^{n+1}\middle|\psi_k^n\right\rangle\neq\delta_{m,k}$. This scheme is not stable since the modulus of the wave-function, $\sqrt{1+\Omega^2\,E_k^2}$, increases with time step. However, one can write a predictor-corrector scheme by introducing a calculation of the wave-function in half time-step. First, the predictor coefficients, $c_{m,p}^{n+1}$, can be found from (23). Next, the corrector coefficients will be given from the expression:

$$c_m^{n+1}=c_k^n\left\langle\psi_m^{n+1}\middle|\psi_k^n\right\rangle(1+\frac{\Omega}{2}E_k^n)+\frac{\Omega}{2}E_m^{n+1}c_{m,p}^{n+1} \tag{24}$$

The general form of this predictor-corrector scheme can be written as follows:

$$\left|\psi^{n+1}\right\rangle(1-\frac{\Omega}{2}E^{n+1})=\left|\psi^n\right\rangle(1+\frac{\Omega}{2}E^n) \tag{25}$$

and one can see that assuming such small Δt, in order for $E^{n+1}\approx E^n$, it preserves the norm. In other words, this scheme is stable for a sufficiently small time step. For structures where the eigen-energies do not change significantly with time, which is the case of the system under study, the suggested methodology can provide an accurate approximation of the time evolution.

VI. TOWARDS TWO-ELECTRON INTERACTION

In the last section of the paper we illustrate how to describe the electrostatic interaction between two electrons, which is essential for the construction of quantum gates. The model under study here is as follows. There is a system of two

double-well cells, each containing one electron. The two cells are separated by some distance. We assume that the electrons are confined to their respective cells. In the first approach, one can treat the Coulomb interaction between the electrons as a perturbation to the effective potential of each confined particle. As we shall see, this pertubative interaction will be sufficient to enforce the particles to occupy a certain state.

Following the logical flow of the paper, we begin by introducing the Schrödinger formalism first, thus capturing physics from first principles. This allows us to track the evolution of each particle in terms of the spatial distributions of their probability densities. However, as a trade-off, we note that the Schrödinger formalism for the two electrons has a perturbative nature.

In order to validate the perturbative interaction in the Schrödinger formalism, we then develop another model using the tight-binding approach. While the tight-binding formalism does not allow to track the spatial distribution of the electrons' wave-functions, it can be easily re-scaled to a large number of interacting particles. In addition, the tight-binding formalism is not perturbative. Having the two different models of interaction, we can make comparisons which conclude that their behaviors are qualitatively very similar. Hence, depending on the task at hand—fast calculations of many-particle problems or more detailed calculations of probability densities—the more appropriate model can be used.

A. INTERACTION MODEL BETWEEN TWO PARTICLES IN TWO DOUBLE QUANTUM WELLS IN THE SCHRÖDINGER FORMALISM

In this section we demonstrate the applicability of the time-dependent predictor-corrector numerical scheme through a preliminary simplified description of weak interaction and quantum correlation between two particles. For this purpose, we will consider two electrons trapped in two separated double wells at a given arbitrary distance [see Fig. 12(a)], such that their Coulomb's interaction is significantly weaker than the potential of each double well. In a simplified view, this can be imagined as two classical charged balls attached to springs and interacting electrostatically. Such particles will oscillate in a way that minimizes their electrostatic energy so that they exhibit anti-correlation in their positions. In our system, instead of the springs, we have a confining potential landscape in which the electron wave-packet moves. We can transfer this picture to a quantum situation where each of oscillating balls will have, for example, a superposition of two eigen-modes referring to two energy eigen-values for each interacting particle. The anti-correlation of oscillations is expected to occur both in classical and quantum pictures. It is therefore expected that we might obtain entangled states in our system when we consider the interaction of many qubits implemented by electrons sitting in certain quantum dots. This is significant as it opens up a possibility of implementing the position-based qubits in CMOS.

In the above case, the mutual electron-electron interaction should not change the electrons' occupancy oscillations

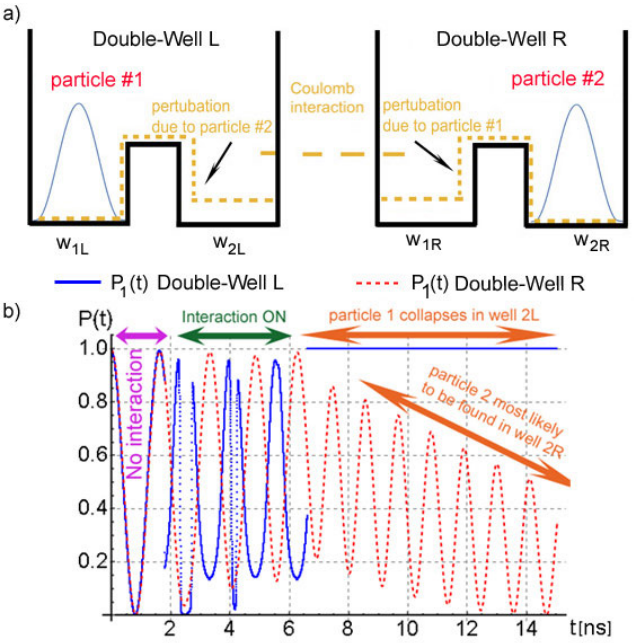

FIGURE 12. (a) Two interacting particles trapped in their respective double-wells. (b) Time evolution of the two interacting particles: Initially, the two particles do not interact and then start evolving from the same initial conditions and with the same phase. After we initiate the interaction, their relative probabilities to be found in the neighbouring wells of the respective double-wells are anti-correlated and we observe a phase-shift. When we force particle #1 to exist on the second well of Double-Well L (w_{2L}), particle #2 is eventually localized on the second well of Double-Well R (w_{2R}).

dramatically as they are governed by the local confining potential. However, the perturbative electron-electron interaction will synchronize the oscillations in a way that they will minimize the global potential energy of electrostatic interaction. At the first stage, we will ignore the occurrence of spin and assume the bosonic system of two particles. Therefore, we will implement the Hartee mean field approach [69] where the occurrence of many bodies is represented by their effective field (effective potential). Assuming a weak mutual interaction between electrons, we can factorize their many-body wave-function as follows:

$$\psi(x_1, x_2, t) = \psi(x_1, t)\psi(x_2, t). \tag{26}$$

The factorization of the two-particle wave-function $\psi(x_1, x_2, t)$ by the two one-particle wave-functions $\psi(x_1, t)$ and $\psi(x_2, t)$ means that the two particles are essentially independent and their mutual interaction has a perturbative nature. It is quite straightforward to extend this scheme to N perturbatively interacting particles. In this model, the Hamiltonian of the system can be written as $H(t) = H_1(t) + H_2(t)$ where $H_1(t)$ is the Hamiltonian of particle #1 and $H_2(t)$ is that of particle #2. Then, each particle is described by a time-dependent Hamiltonian where the effective potential energy will be the potential of the double-well with a small correction due to the presence of the field of the other particle. We can now write an iterative algorithm, which describes the system dynamics as follows:

1) Assume a system of two particles [see Fig. 12(a)]. Particle #1 is trapped in a double-well (in this example denoted as left double-well (Double-Well L)) and particle #2 is trapped in a second double-well (in this example on its right denoted as Double-Well R)). Initially, the two particles do not interact, displaying occupancy oscillations. Particle #1 is described with the Hamiltonian: $H_1(x_1, t) = -\frac{\hbar^2}{2m_1^*}\frac{\partial^2}{\partial x_1^2} + U_{\text{eff1}}(x_1, t)$. Particle #2 is described with the Hamiltonian: $H_2(x_2, t) = -\frac{\hbar^2}{2m_2^*}\frac{\partial^2}{\partial x_2^2} + U_{\text{eff2}}(x_2, t)$. These expressions are dimensionless, and $U_{\text{eff}}(x, t)$ is the effective potential. For indentical particles, $m_1^* = m_2^* = m^*$.
2) After an arbitrary time, when two particles are at a far distance (the average position of each particle is separated by a large distance), initiate their Coulomb interaction.
3) Calculate the effective potential of particle #1 due to the field of particle #2 as: $U_{\text{eff}}(x_1, t) = U_1(x_1) + \int_{-\infty}^{\infty} k_e e^- \frac{|\psi_2(x_2,t)|^2}{|x_1 - x_2|} dx_2$, where $U_1(x_1)$ is the static potential due to double-well 1, k_e is the Coulomb's constant, and e^- is the electronic charge.
4) For the calculated effective potential, consider the Hamiltonian $H_1(t)$ and perform a time step for a given arbitrary small time dt for particle #1 with the predictor-corrector numerical scheme to evaluate the wave-function $\psi(x_1, t + dt)$.
5) Calculate the effective potential of particle #2 due to the field of particle #1 in the same manner.
6) Evaluate the time evolution of particle #2 with the predictor-corrector method.
7) Repeat 1-6.

In Fig. 12(b), we visualize the implementation outcome of this algorithm. Initially, the two particles exist in their respective wells. We initiate occupancy oscillations for the same initial conditions and without considering any interaction. Next, we suddenly activate their Coulomb interaction. This results in a clearly visible instantaneous phase-shift between the probability evolution of the two particles. In particular, they will be anti-correlated. After that, we force particle #1 to stay in w_{2L}. Then, the probability of particle #2 to be found in w_{1R} decreases, i.e. particle #2 will be likely found in w_{2R}.

B. INTERACTION MODEL BETWEEN TWO PARTICLES IN TWO DOUBLE-QUANTUM-WELL SYSTEM IN THE TIGHT-BINDING FORMALISM

The Schrödinger formalism, as already mentioned, provides a continuous-space representation of the wave-function. However, for an electron transport in discrete lattices of structures of different materials and moving towards multiple-interaction particle problems is computationally inefficient. In this section we will describe a non-perturbative tight-binding approach for the system of two interacting quantum double-dots interacting via Coulomb forces (see Fig. 13). This approach can be extended in a straightforward way to many-particle problems.

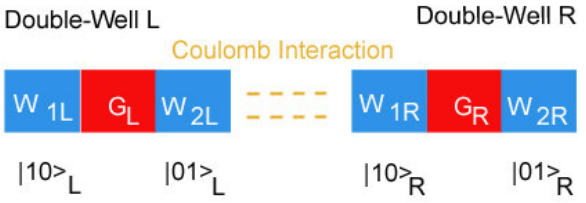

FIGURE 13. Two interacting double-wells in the tight-binding formalism. One double-well is labelled as Left (L) while the other as Right (R). There are two electrons, each occupying their respective double-well cell and interacting through Coulomb's force.

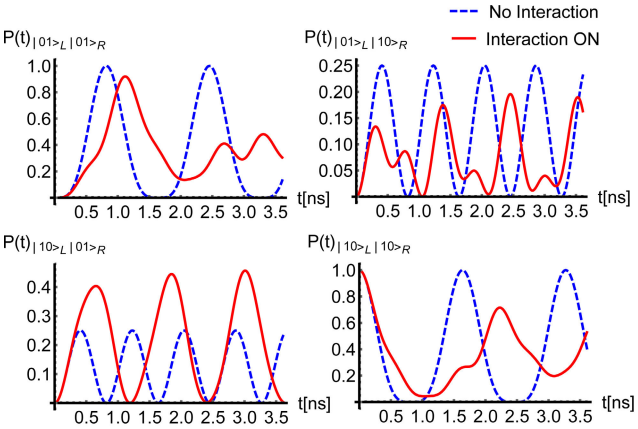

FIGURE 14. Evolution of four quantum states for two non-interacting electrons (dashed blue line) and two interacting electrons (solid red line) in two double-well cells described by the tight-binding formalism.

The wave-function of the two-electron system under study is now presented as follows:

$$|\psi(t)\rangle = a_1(t)\,|10\rangle_L\,|10\rangle_R + a_2(t)\,|10\rangle_L\,|01\rangle_R + a_3(t)\,|01\rangle_L\,|10\rangle_R + a_4(t)\,|01\rangle_L\,|01\rangle_R \quad (27)$$

To understand this notation, refer to Fig. 13. For example, the function $|10\rangle_L\,|10\rangle_R$ denotes the state where particle #1 is found in well #1 of the left double-well and particle #2 is found in well #1 of the right double-well. The relevant coefficients of the four orthogonal states are denoted as a_k with $k = 1, \ldots, 4$ and $\sum_k |a_k|^2 = 1$.

The Hamiltonian operator in matrix representation in this case becomes

$$\hat{\mathrm{H}} = \begin{bmatrix} E_{p11} & t^R_{s2\to1} & t^L_{s2\to1} & 0 \\ t^R_{s,1\to2} & E_{p22} & 0 & t^L_{s2\to1} \\ t^L_{s,1\to2} & 0 & E_{p33} & t^R_{s,2\to1} \\ 0 & t^L_{s,1\to2} & t^R_{s,1\to2} & E_{p44} \end{bmatrix} \quad (28)$$

where $E_{p11} = E^L_{p1} + E^R_{p1} + E^{LR}_{C11}$, $E_{p22} = E^L_{p1} + E^R_{p2} + E^{LR}_{C12}$, $E_{p33} = E^R_{p1} + E^L_{p1} + E^{LR}_{C21}$, $E_{p44} = E^R_{p2} + E^L_{p2} + E^{LR}_{C22}$. In the expression for potential energy, E_p denotes the bottom of the potential well (can be set to zero), and E_c denotes the strength of Coulomb's interaction. Off-diagonal elements in this matrix contain the tunneling-rate (hopping) terms t_s describing the transitions between the wells. In the tight-

binding model, it is more convenient to write the set of linear differential equations on the coefficients $\mathbf{a}(t) = (a_k(t))^T$:

$$i\hbar \frac{d\mathbf{a}(t)}{dt} = \hat{\mathrm{H}}\,\mathbf{a}(t) \tag{29}$$

that can be solved easily, either analytically or numerically. Plugging in the coefficients $\mathbf{a}(t)$ in Eq. (27), one obtains the evolution of the states in this system. Figure 14 shows the time evolution of the four eigen-states of the system. This simulation begins from the state $|10\rangle_L\,|10\rangle_R$ and the two particles experience quite complex occupancy oscillations. For comparison, the occupancy oscillations of the two electrons, each in their respective double-well potential, in the case they do not interact, are shown in the same figure by the dashed lines.

The interpretation of the two-particle system, described by the combined wave-functions, may not seem very straightforward as in the case of the Schrödinger formalism. For example, the localization of particle #1 in the left double-well cell is described not only by the state $|10\rangle_L\,|10\rangle_R$, but also by the state $|10\rangle_L\,|01\rangle_R$. Hence, the probability of such a state is given by $|a_1|^2 + |a_2|^2$.

At this stage, it would be interesting to compare the results that follow from the tight-binding formalism with the results we obtained from the Schrödinger formalism. In the Schrödinger formalism, Fig. 13 shows the dynamics of particle #1 when particle #2 is situated in well #1 of the right double-well (or equivalently, as shown in simulations of Fig. 12, the dynamics of particle #2 when particle #1 is situated in well #2 of the left double-well). As expected, we observe that particle #1 tends to be in well #1 of the left double-well, as far away from particle #2 as possible in this geometry (or in the case that particle #1 is situated in well #2 of the left double-well particle #2 tends to be in well #2 of the right double-well).

In the tight-binding formalism, in order to observe a similar result, we plot the probability of particle #2 to occupy well #1 of the right double-well. We expect that in this case it would be more likely for particle #1 to occupy well #1 of the left double-well (again, be as far away as possible) and less likely to occupy well #2. Figure 15 shows the evolution of the occupancy of well #1 by particle #2. The occupancy of well #1 by particle #1 is clearly correlated with particle #2 while the occupancy of well #2 is clearly anti-correlated. This means that, as shown in Fig. 15, it is more likely to find the two electrons far away apart and least likely to find them in the closest wells. This result is in complete agreement with the result we obtained in the previous section using the Schrödinger formalism.

We conclude that the two models of interaction, the Schrödinger formalism and the tight-binding formalism, are consistent with each other. However, they accentuate different physical aspects of the system. While the Schrödinger formalism provides more insight into the physics of the system, the tight-binding formalism is much more convenient to describe interaction between many-particles.

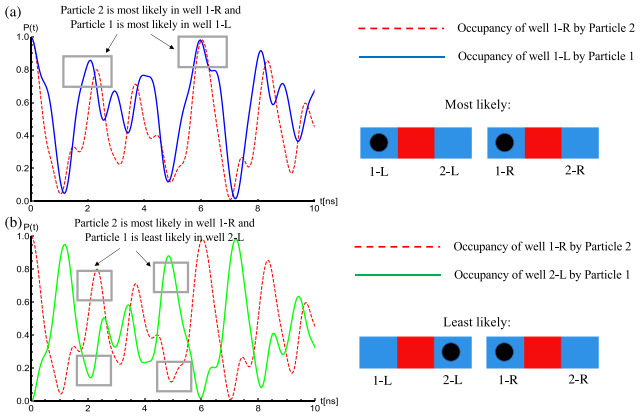

FIGURE 15. (a) Correlation between the occupancy of well #1 by particle #2 in the right double well and the occupancy of well #1 by particle #1 in the left double well (i.e. state $|10\rangle_L\,|10\rangle_R$). (b) Anti-correlation between the occupancy of well #1 by particle #2 in the right double well and the occupancy of well #2 by particle #1 in the left double well (i.e. state $|01\rangle_L\,|10\rangle_R$). If particle #2 is found in well #1 of the right double-well, the most likely configuration for particle #1 is to be in well #1 and the least likely is to be in well #2.

VII. CONCLUSIONS

This study presents a methodology to model electrostatically controlled quantum dots and confirms that they indeed can be seen as artificial atoms and potentially used to construct quantum bits (qubits). The positional-based qubit structure appears amenable to the nanometer-scale CMOS technology which features a very low level of impurities, thus promoting longer decoherence times, and can further isolate the qubits via FD-SoI and FinFET technological options. The system can be treated analytically for the case of time-dependent Hamiltonians by solving the Schrödinger equation with a piece-wise 1D potential, or by employing a tight binding method. This allows to find the dynamically changing Schrödinger wave-packet, its eigen-wave-functions and eigen-energies of the system. Consequently, we can compute the frequency of occupancy oscillations and the temporal dependence of decoherence of a quantum state. The results can allow reducing the delocalization effects present in quantum structures. Moreover, we provide a semi-analytical numerical scheme, demonstrating phenomenologically that quantum correlation is possible for such a system with only a weak electrostatic interaction of two electrons. We also develop a non-pertubative tight binding method for the electron-electron interaction which can be extended, in a straightforward way, to multiple-electron systems.

VIII. ACKNOWLEDGMENT

The authors would like to thank Dr. Andrew Mitchell and Ms. Hongying Wang for fruitful technical discussions. *(Panagiotis Giounanlis and Elena Blokhina contributed equally to this work.)*

REFERENCES

[1] L. Vandersypen and A. van Leeuwenhoek, "Quantum computing the next challenge in circuit and system design," in *Proc. IEEE Int. Solid-State Circuits Conf. (ISSCC)*, Feb. 2017, pp. 24–29.

[2] A. Trabesinger, "Quantum computing: Towards reality," *Nature*, vol. 543, no. 7646, pp. S1–S1, Mar. 2017.

[3] S. Satyajit, K. Srinivasan, B. K. Behera, and P. K. Panigrahi, "Nondestructive discrimination of a new family of highly entangled states in IBM quantum computer," *Quantum Inf. Process.*, vol. 17, no. 9, p. 212, Sep. 2018.

[4] D. Ghosh, P. Agarwal, P. Pandey, B. Behera, and P. Panigrahi. (2017). "Automated error correction in ibm quantum computer and explicit generalization." [Online]. Available: https://arxiv.org/abs/1708.02297

[5] C. W. Lai *et al.*, "Coherent zero-state and p-state in an exciton-polariton condensate array," *Nature*, vol. 450, pp. 529–532, Nov. 2007.

[6] H. Zappe, "Josephson quantum interference computer devices," *IEEE Trans. Magn.*, vol. 13, no. 1, pp. 41–47, Jan. 1977.

[7] K. Pomorski and A. Bednorz, "Justification of the canonical quantization of the josephson effect and its modifications due to high capacitance energy," *J. Phys. A, Math. Theor.*, vol. 49, no. 12, 2016, Art. no. 125002.

[8] N. M. Linke *et al.*, "Experimental comparison of two quantum computing architectures," *Proc. Nat. Acad. Sci. USA*, vol. 114, no. 13, pp. 3305–3310, 2017.

[9] K. Saeedi *et al.*, "Room-temperature quantum bit storage exceeding 39 minutes using ionized donors in silicon-28," *Science*, vol. 342, no. 6160, pp. 830–833, Nov. 2013.

[10] S. E. Thompson and S. Parthasarathy, "Moore's law: The future of Si microelectronics," *Mater. Today*, vol. 9, no. 6, pp. 20–25, 2006.

[11] R. D. Isaac, "Future of nano CMOS technology," *IBM J. Res. Develop.*, vol. 44, no. 3, pp. 369–378, Feb. 2000.

[12] P. Giounanlis, E. Blokhina, D. Leipold, and R. B. Staszewski, "Occupancy oscillations and electron transfer in multiple-quantum-dot qubits and their circuit representation," in *Proc. 25th IEEE Int. Conf. Electron. Circuits Syst. (ICECS)*, Dec. 2018, pp. 1–4.

[13] B. Patra *et al.*, "Cryo-CMOS circuits and systems for quantum computing applications," *IEEE J. Solid-State Circuits*, vol. 53, no. 1, pp. 309–321, Jan. 2018. doi: 10.1109/JSSC.2017.2737549.

[14] B. Szafran, D. Z. ebrowski, and A. Mreńca-Kolasińska, "Electrostatic quantum dots in silicene," *Sci. Rep.*, vol. 8, no. 1, p. 7166, May 2018.

[15] S. Ihara, A. Andreev, D. A. Williams, T. Kodera, and S. Oda, "Quantum dots in single electron transistors with ultrathin silicon-on-insulator structures," *Appl. Phys. Lett.*, vol. 107, no. 1, p. 013102, 2015.

[16] D. Loss and D. P. DiVincenzo, "Quantum computation with quantum dots," *Phys. Rev. A, Gen. Phys.*, vol. 57, no. 1, p. 120, 1998.

[17] M. Rashidi *et al.*, "Initiating and monitoring the evolution of single electrons within atom-defined structures," *Phys. Rev. Lett.*, vol. 121, no. 16, Oct. 2018, Art. no. 166801.

[18] E. Kawakami *et al.*, "Electrical control of a long-lived spin qubit in a Si/SiGE quantum dot," *Nature Nanotechnol.*, vol. 9, no. 9, p. 666, Sep. 2014.

[19] J. J. Pla *et al.*, "A single-atom electron spin qubit in silicon," *Nature*, vol. 489, no. 7417, p. 541, 2012.

[20] R. Vrijen *et al.*, "Electron-spin-resonance transistors for quantum computing in silicon-germanium heterostructures," *Phys. Rev. A, Gen. Phys.*, vol. 62, no. 1, Jan. 2000, Art. no. 012306.

[21] K. K. Likharev, "Single-electron devices and their applications," *Proc. IEEE*, vol. 87, no. 4, pp. 606–632, Apr. 1999.

[22] C. Wasshuber, *Computer Single Electronics*. New York, NY, USA: Springer, 2001.

[23] A. Jain, A. Ghosh, N. B. Singh, and S. K. Sarkar, "A new SPICE macro model of single electron transistor for efficient simulation of single-electronics circuits," *Analog Integr. Circuits Signal Process.*, vol. 82, no. 3, pp. 653–662, Jan. 2015.

[24] E. Doha, A. Bhrawy, M. Abdelkawy, and R. A. V. Gorder, "Jacobi-Gauss-Lobatto collocation method for the numerical solution of $1 + 1$ nonlinear Schrödinger equations," *J. Comput. Phys.*, vol. 261, pp. 244–255, Mar. 2014.

[25] N. Amin and B. Wong, "A study of numerical solutions of the time-dependent Schrödinger equation," *AIP Conf. Proc.*, vol. 1682, no. 1, 2015, Art. no. 020042.

[26] J. Avron and A. Elgart, "The adiabatic theorem of quantum mechanics," *J. Phys. A, Math. Gen.*, vol. 13, no. 2, p. L15, 1998.

[27] T. Hey, "Quantum computing: An introduction," *Comput. Control Eng. J.*, vol. 10, no. 3, pp. 105–112, Jun.1999.

[28] E. Rieffel and W. Polak, "An introduction to quantum computing for non-physicists," *ACM Comput. Surv.*, vol. 32, no. 3, pp. 300–335, Sep. 2000.

[29] M. A. Nielsen and I. Chuang, *Quantum Computation and Quantum Information*. Cambridge, U.K.: Cambridge Univ. Press, 2002. [Online]. Available: http://mmrc.amss.cas.cn/tlb/201702/W020170224608149940643.pdf

[30] E. Kolley and W. Kolley, "Collective action formalism on the Keldysh contour for disordered and hubbard-correlated electrons," *Phys. Status Solidi B*, vol. 145, no. 2, pp. 585–596, Feb. 1988.

[31] N. Friis *et al.*, "Observation of entangled states of a fully controlled 20-qubit system," *Phys. Rev. X*, vol. 8, no. 2, 2018, Art. no. 021012.

[32] S. Debnath, N. M. Linke, C. Figgatt, K. A. Landsman, K. Wright, and C. Monroe, "Demonstration of a small programmable quantum computer with atomic qubits," *Nature*, vol. 536, no. 63, p. 63, Aug. 2016.

[33] M. Russ and G. Burkard, "Three-electron spin qubits," *J. Phys. Condensed Matter*, vol. 29, no. 39, 2017, Art. no. 393001.

[34] X.-Y. Zhu, T. Tu, A.-L. Guo, Z.-Q. Zhou, C.-F. Li, and G.-C. Guo, "Dynamics of probing a quantum-dot spin qubit with superconducting resonator photons," *Sci. Rep.*, vol. 8, no. 1, 2018, Art. no. 15761.

[35] T. Fujisawa, T. Hayashi, H. D. Cheong, Y. H. Jeong, and Y. Hirayama, "Rotation and phase-shift operations for a charge qubit in a double quantum dot," *Phys. E, Low-Dimensional Syst. Nanostruct.*, vol. 21, nos. 2–4, pp. 1046–1052, 2004.

[36] G. Shinkai, T. Hayashi, T. Ota, and T. Fujisawa, "Correlated coherent oscillations in coupled semiconductor charge qubits," *Phys. Rev. Lett.*, vol. 103, Jul. 2009, Art. no. 056802.

[37] K. D. Petersson, J. R. Petta, H. Lu, and A. C. Gossard, "Quantum coherence in a one-electron semiconductor charge qubit," *Phys. Rev. Lett.*, vol. 105, no. 24, p. 246804, Dec. 2010.

[38] A. Weichselbaum and S. Ulloa, "Charge qubits and limitations of electrostatic quantum gates," *Phys. Rev. A, Gen. Phys.*, vol. 70, no. 3, 2004, Art. no. 032328.

[39] S. Y. Nakamura and A. Pashkin, "Coherent control of macroscopic quantum states in a single-cooper-pair box," *Nature*, vol. 398, no. 6730, p. 786, 1999.

[40] D. P. K. Bladh and T. Duty, "The single cooper-pair box as a charge qubit," *New J. Phys.*, vol. 7, no. 1, p. 180, Aug. 2005.

[41] R. M. Lutchyn, Ł. Cywiński, C. P. Nave, and S. Das Sarma, "Quantum decoherence of a charge qubit in a spin-fermion model," *Phys. Rev. B, Condens. Matter*, vol. 78, no. 2, Jul. 2008, Art. no. 024508.

[42] D. Kwiatkowski and Ł. Cywiński, "Decoherence of two entangled spin qubits coupled to an interacting sparse nuclear spin bath: Application to nitrogen vacancy centers," *Phys. Rev. B, Condens. Matter*, vol. 98, Oct. 2018, Art. no. 155202.

[43] J. Q. You and F. Nori, "Superconducting circuits and quantum information," *Phys. Today*, vol. 58, no. 11, pp. 42–47, 2005.

[44] D. Yu, M. M. Valado, C. Hufnagel, L. C. Kwek, L. Amico, and R. Dumke, "Charge-qubit–atom hybrid," *Phys. Rev. A, Gen. Phys.*, vol. 93, Apr. 2016, Art. no. 042329.

[45] J. A. Schreier *et al.*, "Suppressing charge noise decoherence in superconducting charge qubits," *Phys. Rev. B, Condens. Matter*, vol. 77, May 2008, Art. no. 180502.

[46] M. Gonzalez-Zalba. (2018). "Solid state qubits." [Online]. Available: https://arxiv.org/abs/1801.06722

[47] G. D. Éthier-Majcher *et al.*, "Improving a solid-state qubit through an engineered mesoscopic environment," *Phys. Rev. Lett.*, vol. 119, Sep. 2017, Art. no. 130503.

[48] T. Stievater *et al.*, "Rabi oscillations of excitons in single quantum dots," *Phys. Rev. Lett.*, vol. 87, no. 13, 2001, Art. no. 133603.

[49] S. Datta, *Quantum Transport: Atom to Transistor*. Cambridge, U.K.: Cambridge Univ. Press, 2005.

[50] G. Brocks, "Electron transport at the nanoscale lecture notes, preliminary version," Tech. Rep., 2005. [Online]. Available: https://scholar.google.com/scholar?cluster=7484487599246789085&hl=en&as_sdt=0,5

[51] K. D. Pomorski, H. Akaike, A. Fujimaki, and K. Rusek, "Relaxation method in description of ram memory cell in rsfq computer," *Int. J. Comput. Math. Electr. Electron. Eng.*, vol. 38, no. 1, pp. 395–414, 2019.

[52] J. Killingbeck, "Shooting methods for the schrodinger equation," *J. Phys. A, Math. Gen.*, vol. 20, no. 6, p. 1411, 1987.

[53] T. Fujisawa, T. Hayashi, R. Tomita, and Y. Hirayama, "Bidirectional counting of single electrons," *Science*, vol. 312, no. 5780, pp. 1634–1636, 2006.

[54] E. Peacock-Löpez, "Exact solutions of the quantum double square well potential," *Chem. Educator*, vol. 11, pp. 383–393, 2006.
[55] P. Vogl, H. P. Hjalmarson, and J. D. Dow, "A Semi-empirical tight-binding theory of the electronic structure of semiconductors," *J. Phys. Chem. Solids*, vol. 44, no. 5, pp. 365–378, Jun. 1983.
[56] H. Xu, "Method of calculations for electron transport in multiterminal quantum systems based on real-space lattice models," *Phys. Rev. B, Condens. Matter*, vol. 66, no. 16, 2002, Art. no. 165305.
[57] R. R. Parwani *et al.*, "Can degenerate bound states occur in one-dimensional quantum mechanics?" *EPL Europhys. Lett.*, vol. 80, no. 3, 2007, Art. no. 30004.
[58] J. D. Kelley and J. J. Leventhal, *Problems in Classical and Quantum Mechanics: Extracting the Underlying Concepts*. New York, NY, USA: Springer, 2017.
[59] V. Bargmann, "On the number of bound states in a central field of force," *Proc. Nat. Acad. Sci. United States Amer.*, vol. 38, no. 11, p. 961, Aug. 1952.
[60] N. Marzari, "Maximally localized wannier functions: Theory and applications," *Rev. Modern Phys.*, vol. 84, no. 4, p. 1419, 2012.
[61] D. J. Griffiths, *Introduction to quantum mechanics*. Cambridge, U.K.: Cambridge Univ. Press, 2016.
[62] D. Rotta, F. Sebastiano, E. Charbon, and E. Prati, "Quantum information density scaling and qubit operation time constraints of cmos silicon-based quantum computer architectures," *NPJ Quantum Inf.*, vol. 3, no. 1, p. 26, Jun. 2017.
[63] F. Marquardt and A. Püttmann. "Introduction to dissipation and decoherence in quantum systems." [Online]. Available: https://arxiv.org/abs/0809.4403
[64] J. Gorman, D. Hasko, and D. Williams, "Charge-qubit operation of an isolated double quantum dot," *Phys. Rev. Lett.*, vol. 95, no. 9, 2005, Art. no. 090502.
[65] E. Paladino, Y. Galperin, G. Falci, and B. Altshuler, "1/f noise: Implications for solid-state quantum information," *Rev. Modern Phys.*, vol. 86, no. 2, p. 361, Jun. 2014.
[66] P. Kushwaha *et al.*, "A unified flicker noise model for FDSOI MOSFETs including back-bias effect," in *Proc. IEEE Int. Conf. Electron., Comput. Commun. Technol. (CONECCT)*, Mar. 2018, pp. 1–5.
[67] J. Bergli, Y. M. Galperin, and B. Altshuler, "Decoherence in qubits due to low-frequency noise," *New J. Phys.*, vol. 11, no. 2, 2009, Art. no. 025002.
[68] Y. Utsumi. (2006). "Full counting statistics for number of electrons dwelling in a quantum dot." [Online]. Available: https://arxiv.org/abs/cond-mat/0604082
[69] J. C. Slater, "A simplification of the hartree-fock method," *Phys. Rev.*, vol. 81, pp. 385–390, Feb. 1951.

PANAGIOTIS GIOUNANLIS received the B.Sc. degree in physics, the M.Sc. degree in computational physics from Aristotle University of Thessaloniki, Greece, in 2008 and 2011, respectively, and the Ph.D. degree for his research on the modeling of non-linear effects for micro-scale devices and their application to reliability and control by the use of both numerical and analytical approaches, in 2017.

He has been a Postdoctoral Researcher with University College Dublin, since 2017. His current work includes the development of numerical and analytical approaches for the modeling and simulation of nano-structures and semi-conductor-coupled quantum-dots, the development of circuit equivalent models for electron transfer through multiple-quantum-dots, and the characterization and modeling of CMOS devices operation at low temperatures and others. His research interests include modeling and simulation of micro/nano-scale devices and mixed domain complex systems, solid state physics, and computational quantum mechanics.

ELENA BLOKHINA (S'05–M'06–SM'13) received the M.Sc. degree in physics and the Ph.D. degree in physical and mathematical sciences from Saratov State University, Russia, in 2002 and 2006, respectively, and the Habilitation HDR degree in electronic engineering from UPMC Sorbonne Universities, France, in 2017. From 2005 to 2007, she was a Research Scientist with Saratov State University. Since 2007, she has been with the School of Electrical and Electronic Engineering, University College Dublin, Ireland, where he is currently a Lecturer and the Coordinator of the Circuits and Systems Research Group. Her research interests include the analysis, design, modeling, and simulations of nonlinear circuits, systems and networks with particular application to complex, mixed-domain, and multi-physics systems.

Dr. Blokhina is the Chair Elect of the IEEE Technical Committee on Nonlinear Circuits and Systems. She had been elected to serve as a member of the Boards of Governors of the IEEE Circuits and Systems Society, from 2013 to 2015 and has been re-elected, from 2015 to 2017. She has served as a member of organizing committees, review and programme committees, session chair, and track chair at many leading international conferences on circuits, systems, and electronics, including the IEEE International Symposium on Circuits and Systems. She has served as the Programme Co-Chair of the first edition of IEEE Next Generation of Circuits and Systems Conference 2017 and of the IEEE International Conference on Electronics, Circuits and Systems 2018. From 2016 to 2017, she was an Associate Editor of the IEEE TRANSACTIONS ON CIRCUITS AND SYSTEMS I, where she has been the Deputy Editor-in-Chief, since 2018.

KRZYSZTOF POMORSKI received the Ph.D. degree from the Faculty of Physics, Astronomy and Applied Computer Science, Jagiellonian University, Krakow, Poland, in 2015. During his Ph.D. research, he developed the scheme of field-induced Josephson junctions and pointed out the existence of topological Meissner effect. He also developed microscopic justification of canonical quantization of Josephson effect. He is specialized in fundamental modeling of devices with the use of physics methodology and in the development of new numerical algorithms. He held a postdoctoral position working on design of superconducting RAM for fluxon electronics at Nagoya University for 9 months. For one year at the Department of Telecommunication, AGH University of Science and Technology, he was giving lectures on Artificial Intelligence and Artificial Life. At the same time, he was continuing the cryogenic experiments. He currently holds a postdoctoral position with University College Dublin, involved in both quantum simulations and in advanced cryogenic engineering. His interdisciplinary approach is coming from two M.Sc. degrees in theoretical physics from the University of Lodz and in electronics from the Lodz University of Technology, Poland. He is currently involved in the design of hybrid classical-quantum computer and in study of quantum neural networks. The interlink between classical and quantum information theory, many-body physics, quantum field theory, statistical physics is expecting to bring unique synergy between theoretical physics, and the development of new quantum technologies. In particular, it shall boost the development of quantum AI and quantum Artificial Life. His research interests include the implementation of quantum computer in semiconductors and in superconductors, physics of Josephson junctions, semiconductor, and superconducting electronics.

DIRK R. LEIPOLD (M'96) received the Diploma degree in physics from the University of Konstanz, in 1991, and the Ph.D. degree in physics, in 1995. Since 1995, he has been working in semiconductor physics, semiconductor circuits, and semiconductor circuit system design at various semiconductor OEM and start-up companies. He has created more than 150 patents on semiconductor device design, cell phone circuitry, and optical sensor design. He has created innovative circuit concepts, such as the Digital Radio Processor at Texas Instruments, allowing the integration of cell phone radio front-end in a digital CMOS process and the first high volume CMOS power amplifier for cell phones. These products have been deployed in more than 2 billion devices worldwide.

Since 2015, he has been working on a foundry-based SOI-based quantum computer solution based on entangled quantum aperture logic (equal) which allows very dense quantum computer solution implantation as single chip solution. He is currently a CEO of Equal1 Labs, where he has been working on a commercial quantum computer solution based on CMOS technology.

ROBERT BOGDAN STASZEWSKI (M'97–SM'05–F'09) was born in Bialystok, Poland. He received the B.Sc. *(summa cum laude)*, M.Sc., and Ph.D. degrees from The University of Texas at Dallas, Richardson, TX, USA, in 1991, 1992, and 2002, respectively, all in electrical engineering. From 1991 to 1995, he was with Alcatel Network Systems, Richardson, where he was involved in SONET cross-connect systems for fiber optics communications. In 1995, he joined Texas Instruments Incorporated, Dallas, TX, USA, where he was elected as a Distinguished Member of Technical Staff (limited to 2% of technical staff). From 1995 to 1999, he was involved in advanced CMOS read channel development for hard disk drives. In 1999, he co-started the Digital RF Processor (DRP) group within Texas Instruments, Inc., with a mission to invent new digitally intensive approaches to traditional RF functions for integrated radios in deeply scaled CMOS technology. From 2007 to 2009, he was a CTO of the DRP Group. In 2009, he joined the Delft University of Technology, Delft, The Netherlands, where he currently holds a guest appointment of Full Professor *(Antoni van Leeuwenhoek Hoogleraar)*. Since 2014, he has been a Full Professor with the University College Dublin, Dublin, Ireland. He has authored or coauthored four books, five book chapters, 240 journal and conference publications, and holds 170 issued U.S. patents. His current research interests include nanoscale CMOS architectures and circuits for frequency synthesizers, transmitters, receivers, and quantum computers. He is a co-founder of a startup company Equal1 Labs aiming at building the first practical CMOS quantum computer.

Dr. Staszewski was a Technical Program Committee (TPC) Member of the IEEE International Solid-State Circuits Conference, from 2008 to 2012, the IEEE International Symposium on Radio-Frequency Integration Technology, from 2009 to 2014, and the IEEE Radio-Frequency Integrated Circuits Symposium, from 2010 to 2014. He has been a TPC member of the IEEE International Symposium on Circuits and Systems, since 2010 and has also been the IEEE European Solid-State Circuits Conference (ESSCIRC), since 2013. He is a TPC Chair of 2019 ESSCIRC in Krakow, Poland. He was a recipient of the 2012 IEEE Circuits and Systems Industrial Pioneer Award. He was the Chair of the TPC of the IEEE Dallas Circuits and Systems Workshop, from 2005 to 2008.